Journal of Mines, Metals and Fuels, *71(12A): 177-184; 2023. DOI: 10.18311/jmmf/2023/43595*

Print ISSN : 0022-2755

Journal of Mines, Metals and Fuels

Contents available at: *www.informaticsjournals.com/index.php/jmmf*

Study of Structural and Dielectric Properties of Zirconium Titanate ($ZrTiO_4$) Nano Powder

A. Sangeetha[1]*, B. M. Nagabhushana[2], Divyashree[3], Chaitra[3] and Netravathi[3]

[1]Department of Physics, Government First Grade College, Hoskote, Bengaluru - 562114, Karnataka, India; amblisangeetha@gmail.com

[2]Department of Chemistry, M.S. Ramaiah Institute of Technology, Bengaluru, Karnataka, India

[3]Government First Grade College, Yelahanka, Bengaluru - 560064, Karnataka, India

Abstract

Zirconium Titanate nano powders synthesized by Polymeric Precursor Method using glycerin as a polymerizing agent were studied to investigate the effect of sintering temperature on structural and dielectric properties. From XRD reports, it is evident that phase formation is dependent on sintering temperature. UV-Visible Spectroscopy reveals that the band gap of the material depends on the structure that can be controlled by temperature. Variation of Dielectric constant (ε) and dielectric loss (tanδ) of the powders were measured for a wide range of frequency from 100Hz to 5MHz. Conductivity properties such as Conductivity and Impedance were studied for the above said frequency range.

Keywords: *Dielectric Constant, Dielectric Loss, Zirconium Titanate*

1.0 Introduction

Analysis of dielectric properties has become a pivotal area of research in search of new composites that offer extremely high permittivity, low dielectric losses when subjected to high frequencies to meet the needs of applications such as computers, wireless communication and satellite communication. Dielectric resonators, oscillators, capacitors and antennas are fundamental elements of mobile communication, global positioning system and miniaturization technology[1-3]. Metal oxides are found to be appealing for wide range of applications due to their high thermal and chemical stability[4-6]. Although, there are various oxide materials available, suitable for above mentioned applications, zirconium titanate ($ZrTiO_4$) is regarded as an excellent material because of its high dielectric permittivity, low dielectric losses and chemical stability[7,8]. $ZrTiO_4$ is a ceramic having orthorhombic structure similar to α-PbO_2 structure[9]. Morphological dependency of the properties of nano particles has resulted in development of several synthesis techniques. From literature review, it is evident that $ZrTiO_4$ nano particles can be synthesized by physical as well as chemical routes. Choice of synthesis method is based on the nature of the particles essential for explicit application. Research reports reveal that ball milling, sputtering, laser ablation, nanolithography and laser pyrolysis are some of the physical routes available for the preparation of $ZrTiO_4$ nano particles[10-12]. As compared to physical routes, chemical route has become more popular as they yield high quality product. Moreover, readiness to tune the dimensions of the particles by controlling various parameters such as temperature, pressure, PH, synthesis atmosphere etc., is an added advantage of chemical routes. co-precipitation, solvo-thermal, hydrothermal, solgel, polymeric precursor and combustion are some

*Author for correspondence

of the chemical routes reported for the synthesis of $ZrTiO_4$[13-16].

In this work $ZrTiO_4$ nano particles were synthesized by polymeric precursor method. Study reports about the impact of heat treatment on the phase and conductivity properties of $ZrTiO_4$.

2.0 Experimental

2.1 Materials Used

Analytical grade reagents of high purity were used for the synthesis of Zirconium titanate. Zirconium n-propoxide ($C_{12}H_{28}O_4Zr$) (99% pure) from Sigma Aldrich, Titanium isopropoxide ($C_{12}H_{28}O_4Ti$) of SpectraChem (98% pure), citric acid ($C_6H_8O_7$) and glycerin from SpectraChem ($C_3H_8O_3$) were used for synthesis.

2.2 Synthesis Method

In this work, polymeric precursor method is used to synthesize of $ZrTiO_4$. Zirconium and Titanium citrates were prepared by adding zirconium and titanium propoxides to citric acid. Metal oxide and citric acid were taken in the proportion of 3:1. Glycerine is used as a chelating agent. Metal-citrates and glycerine mixture forms a chelate complex. Polyesterification of this complex can be initiated by heating the mixture uniformly at 100 °C for 2 h. This leads to a formation of polymeric network which is then kept in a pre-heated furnace at 300 °C for 1 h to form an expanded resin. Obtained resin material has been grounded using agate and mortar and five different samples were formed by sintering at 500 °C , 600 °C , 700 °C , 800 °C and 900 °C for 2 h. Final product is a white ceramic powder.

2.3 Preparation of Pellets

To carry out dielectric measurements, powdered samples were pelletized using pelletizer. 0.156g of $ZrTiO_4$ powder has been transferred to pelletizer and pressure of about 5 tons has been applied for about 5 minutes to form a circular pellet in the form of disc. Pellets were coated with silver paste to provide electrical connections for dielectric measurements.

2.4 Instruments Used

XRD analysis of the synthesized samples has been carried out using Bruker D8 Advance diffraction system. Fourier Transform Infra-Red (FTIR) spectroscopic measurements has been done using Perkin Elmer instrument. Optical measurements such as absorbance has been recorded from Lambda 385 Perkin Elmer UV-Visible spectrophotometer. Pellets were made from Hydraulic press (Shimazdu, Japan). Dielectric measurements have been recorded from WAYNE KERR 6500B conductivity apparatus.

3.0 Results and Discussion

3.1 X-Ray Diffraction Analysis

Figure 1 show XRD pattern of $ZrTiO_4$ sintered at five different temperatures. Peaks due to all samples are matched with JCPDS file No. 34-0415. All the samples

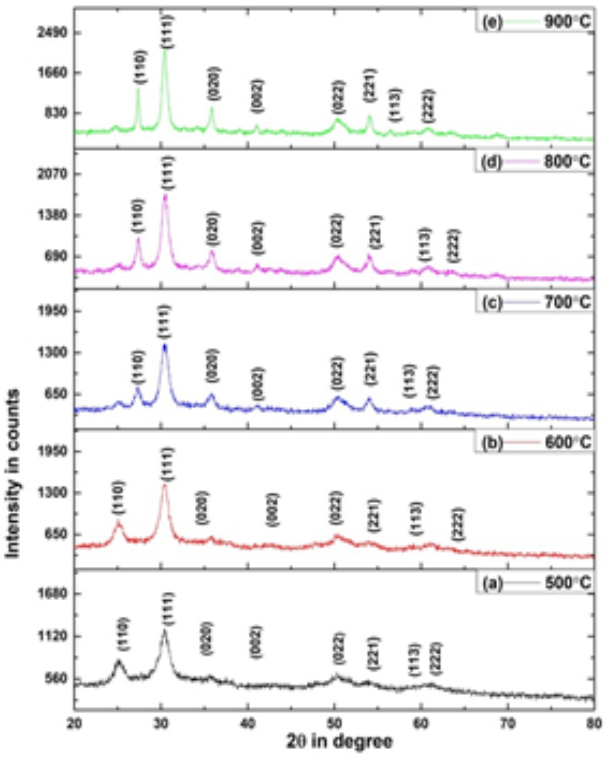

Figure 1. X-Ray diffraction pattern of $ZrTiO_4$.

are in α-PbO_2 orthorhombic structure[15]. From graph it is noticed that height of the peaks enhanced with increasing calcination temperature up to 900 °C. This clearly indicate that percentage of crystallinity is temperature dependent. Change in the intensities in XRD is attributed to the crystallinity of the materials. Due to heat treatment, extent of crystallinity of the sample increased.

Average crystallite size of calcined samples was calculated using Debye Scherrer's formula by considering Full Width Half Maxima (FWHM) of prominent peaks obtained in XRD. Average crystallite size of $ZrTiO_4$ nano powders at 500 °C, 600 °C, 700 °C, 800 °C and 900 °C are found to be 1.953 nm, 2.846 nm, 3.073 nm, 6.743 nm and 6.548 nm respectively. Peak shifting towards higher scattering angle observed in XRD with temperature is related to the structural changes of the synthesized product. Peak shift towards higher angles specify that tensile stress has been introduced due to heat treatment.

3.2 IR Spectroscopy

IR spectra of the samples has been recorded from 350 cm^{-1} to 900 cm^{-1} (Figure 2). Peaks occurred at 3439 cm^{-1} and 1624 cm^{-1} represents stretching vibrations of O-H bonds indicating retention of water content in the samples. Band around 1368 cm^{-1} is concerned to Ti-O-Ti stretching bond, and peaks at 1113 cm^{-1} and 557 cm^{-1} represents Zr-O and Zr-O-Ti groups. IR spectra confirms the formation of $ZrTiO_4$.

3.3 Uv-Visible Spectroscopy

Uv-Visible spectra in absorbance mode has been recorded from 350 to 900 nm (Figure 3). Band gap has been calculated using Tauc's relation. For direct band gap materials absorption coefficient is given by

$$\alpha(h\nu) = B(h\nu - E_g)^m$$

Band gap of the samples varied with respect to calcination temperature. Calculated band gap of $ZrTiO_4$ samples with increasing calcination temperature from 500 °C to 900 °C are accordingly, 3.64 eV, 3.82 eV, 4.07 eV, 4.00 eV and 2.33 eV. These results indicates that increase in the crystallinity up to 700 °C forms a well defined structure without intermediate level between top most valance band and bottom of the conduction band. According to reports, perfect crystallization temperature

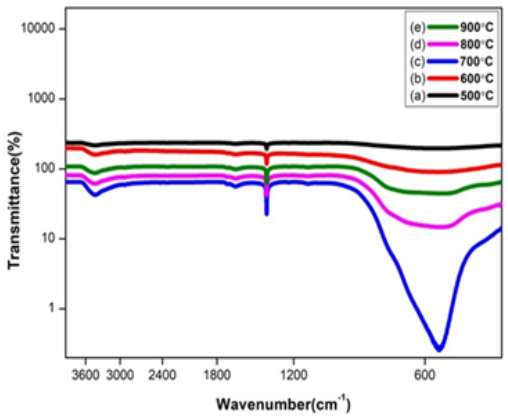

Figure 2. FTIR spectra of $ZrTiO_4$.

of $ZrTiO_4$ is around 700 °C[17,18]. At 800 °C and 900 °C, decomposition of $ZrTiO_4$ into oxides of titanium and zirconium might have occurred and introduced defective levels resulting in the reduction of band gap. No superlattice peaks are observed in XRD which may be due to very low concentration decomposed oxides.

3.4 Dielectric Properties

Frequency dependent dielectric properties of the prepared samples were studied for different sintering temperature. Complex form of dielectric constant is given by $\varepsilon^* = \varepsilon' + i\varepsilon''$, where real or relative part ε' gives the relation between transmission speed of the AC signal and the capacitance of the material. Imaginary part ε'' called as the loss factor refers to the energy loss and measures dissipative power of a material. The dielectric loss tangent (tan δ) of a material signifies electrical energy dissipation as a result of various processes such as conductivity and dielectric relaxation. Impedance is given by $Z^* = Z' + iZ''$, real part Z' represents resistance of the material which measures the dissipated power as a heat. Imaginary part Z" refers to reactance of the material which gives the measure of energy stored in the form of an electric field.

Complex electric modulus 'M' is given by $M^* = M' + iM''$. It corresponds to the relaxation of electric field in the material given by $M^* = 1/\varepsilon^*$. It is another way to analyse frequency response of conductivity and dielectric relaxation of the material that cannot be obtained from impedance graphs. Dielectric parameters of $ZrTiO_4$ have

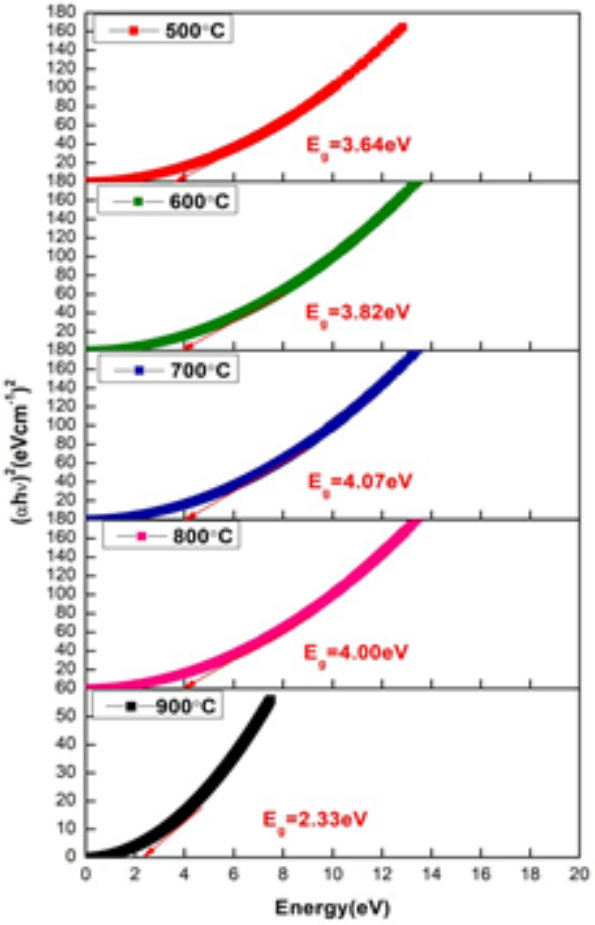

Figure 3. UV-Visible spectra of $ZrTiO_4$

been studied as a function frequency (100 Hz to 5 MHz) at room temperature. Electrodes on either side of the pellets has been provided by coating silver paste.

3.4.1 Dielectric Constant

Figure 4a represents the graph of variation of ε' with respect to frequency. It is evident from graph that ε' decreases rapidly at lower frequency and becomes almost constant at high frequencies. High value of ε' arises due to inhomogeneity in the structure of the material. At lower frequencies material appears to be constituted of large number of conducting grains separated by insulating grain boundaries. This is equivalent to parallel combination of capacitance and resistance that contributes to high value of ε'. This nature of dielectric constant can be explained based on Maxwell-Wagner polarization theory[19,20].

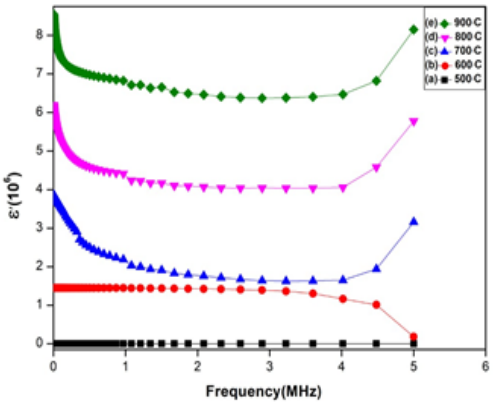

Figure 4a. Variation of ε' as a function of frequency.

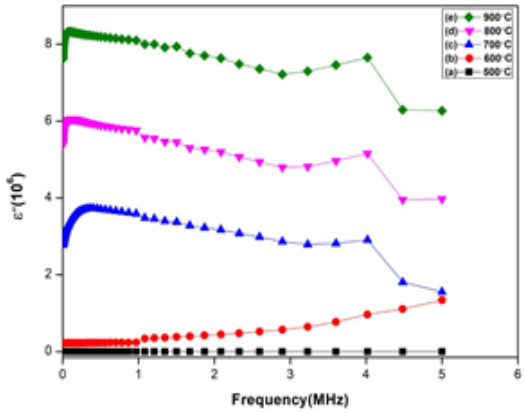

Figure 4b. Variation of ε" of $ZrTiO_4$ as a function of frequency.

At higher frequency region, these conducting grains start predominating the grain boundaries causing decrease in the value of dielectric constant. Both ionic and the electronic polarisation mechanisms contribute to dielectric constant of a material at high frequency of an alternating electric field and resonance phenomena implies for total dielectric constant. Hence a peak appears in the plot of dielectric constant versus frequency, at the resonance frequencies of the ionic and electronic polarisation modes. A dip appears at frequencies just above each resonance peak, which is a general phenomenon of all damped resonance responses, corresponding to the response of the system being out of phase with the driving

force. Further, availability of the polarization mechanisms is structure dependent. Small variation in the crystallinity of the materials as attributed to peak shift in XRD, varies the number of available polarization. Thus variation of the dielectric constant show slightly different behaviour at different calcination temperatures. Frequency dependent variation of imaginary part of dielectric constant ε" shows same behaviour as that of ε'. Values of ε'and ε" increased with increase in the sintering temperature.

3.4.2 Dielectric Loss (Tanδ)

Graph of dielectric loss (Tanδ) with respect to frequency is shown in Figure 5. Tanδ value is maximum at lower frequency and decreases with increasing frequency. At lower frequencies, mechanism of hopping of charges between grains follows the frequency of applied field hence the losses will have maximum value. At higher frequencies, the exchange of charges between adjacent grains does not match the frequency of electric field. Thus the losses decrease. Moreover, tanδ is proportional to imaginary part of dielectric constant and hence shows same nature of variational pattern[21]

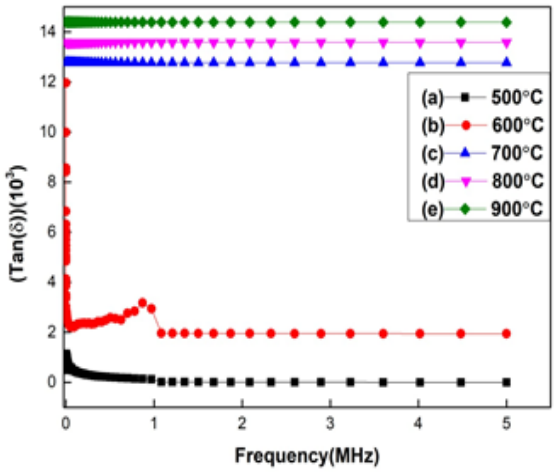

Figure 5. Variation of tanδ as a function of frequency.

3.4.3 AC Conductivity

From Figure 6 we observe that nano composites have a plateau region from low frequency to high frequency region which implies that electrical conductivity is independent of frequency. Value of AC conductivity found to increase with increase in the sintering temperature. High value of conductivity is due to hopping mechanism of carriers over the barrier between the grain and grain boundary.

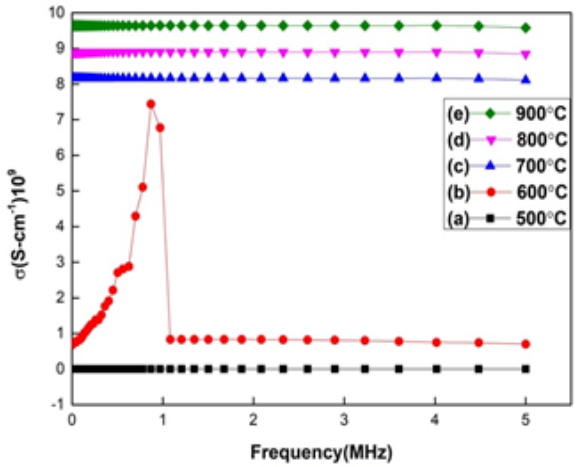

Figure 6. Variation of σ_{ac} as a function of frequency.

3.4.4 Impedance Analysis

Impedance plots with respect to frequency for all sintering temperatures are shown in Figures 7a and 7b. High value of real and imaginary impedances Z′ and Z″ at lower frequency for all temperatures can be attributed to grain boundaries that act as a barrier for conductivity. As the frequency is increased, the value of impedance decreases and becomes independent of frequency which matches with the conductivity behaviour of the samples. The value of impedance increases with respect to increase in the sintering temperature.

Cole-Cole plot of Z′ versus Z″ for all temperatures were plotted in Figure 8 to analyse the significance of grains and grain boundaries on conductivity. Two semi-circular arcs are usually obtained in which, first appearing at lower frequency describes the contribution of grain boundaries and the second at higher frequency describes the contribution of grains for conductivity. All samples exhibit one semi-circular arc except at 700 °C. Single semicircle obtained indicates the contribution of grain boundaries for conductivity[22]. At 700 °C, two arc signify the effect of grain boundaries at lower frequency and grains at higher frequency. This behaviour may be related to structure of the material. It is clear from Cole-Cole

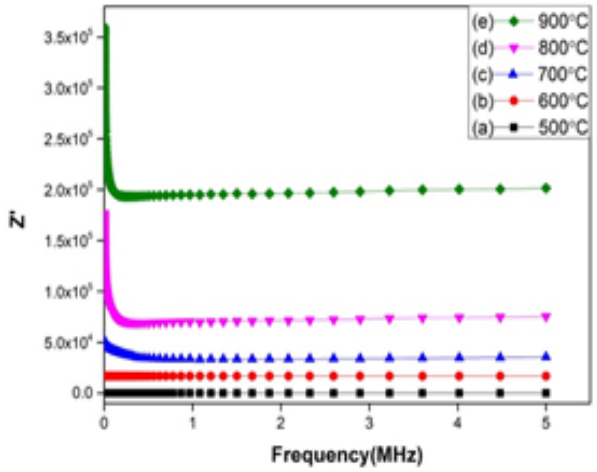

Figure 7a. Variation of Z′ as a function of frequency.

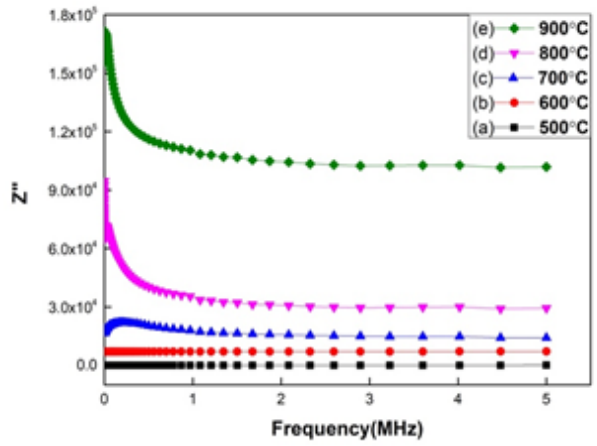

Figure 7b. Plot of Z" of as a function of frequency.

plot that the semi-circular arcs are asymmetric in nature indicating that the relaxation type is non-Debye type with different relaxation times[23].

3.4.5 Electric Modulus

The mechanism concerned conductivity of a material can be analysed from complex electric modulus given by $M = M' + iM''$, where real part of electric modulus is given by relation $M' = \frac{\varepsilon'^2}{\varepsilon'^2 + \varepsilon''^2}$ and imaginary part of the electric modulus given by $M'' = \frac{\varepsilon''^2}{\varepsilon'^2 + \varepsilon''^2}$. Study of

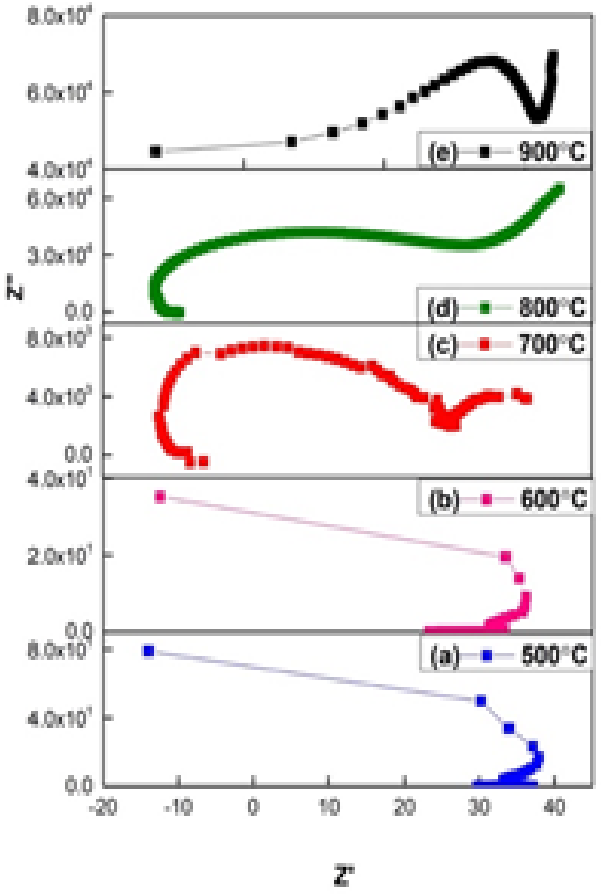

Figure 8. Plot of Z′ versus Z" as a function of frequency.

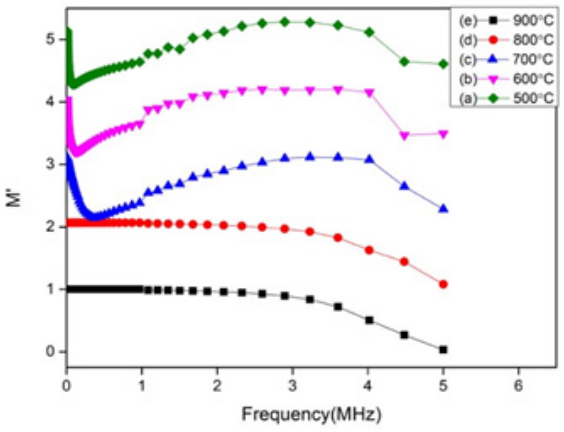

Figure 9a. Plot of M′ versus frequency.

electric modulus helps to know the effect of electrode contribution to dielectric constant. Figures 7a and 7b

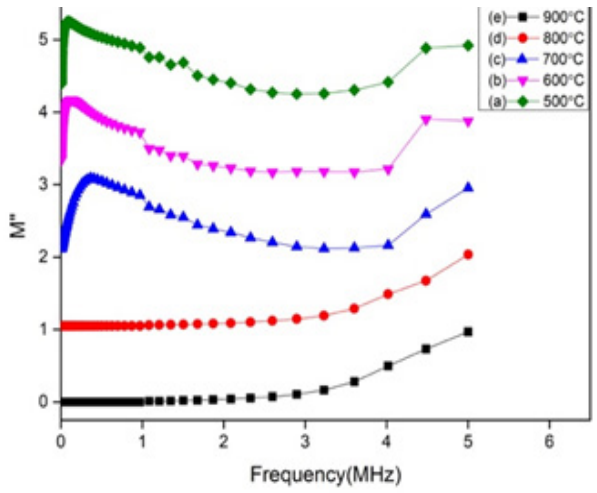

Figure 9b. Plot of M" versus frequency.

depicts graph of M′ and M″ with respect to frequency. High value of M′ and M″ implies the presence of electrode polarization at low frequencies. Saturation of M′ and M″ indicates the expulsion of space charge polarization in the samples[24].

4.0 Conclusion

Zirconium titanate nano powder was synthesized by polymeric precursor method using glycerine as chelating agent. Synthesized powder has been sintered at different temperature for 2 hours to study the effect of heat treatment on the structure and the transport properties. It has been found that the perfect crystalline single phase can be obtained at 700 °C. Band gap of the material found to increase with increase in the sintering temperature and decreased for sintering temperature 800 °C and 900 °C which may be due to decomposition of the compound giving rise to intermediate energy levels. Conductivity studies show that synthesized samples show high dielectric constant and low dielectric loss. AC conductivity, impedance variation and electric modulus were studied from frequency range 100 Hz to 5 MHz from the conductivity analysis it is relevant that synthesized nano powders are best suited for applications such as high storage capacitors, dielectric resonators and size miniaturization devices.

5.0 Acknowledgements

We gratefully acknowledge Department of Collegiate Education and Government First Grade College, Yelahanka for their support undertake this research work, MSRIT Bangalore for providing synthesis, Characterization facilities and human resource for guidance and Dr. Murugendrappa, Department of Physics, BMS Engineering College, Bangalore for extending the facility of dielectric measurements.

6.0 References

1. Vescio G, Crespo-Yepes A, Alonso D, Claramunt S, Porti M, Rodriguez R, Cornet A, Cirera A, Nafria M, Aymerich X. IEEE Electron Device Lett. 2017; 38:457. https://doi.org/10.1109/LED.2017.2668599
2. Mostafa M, Rahman MJ, Choudhury S. Enhanced dielectric properties of $BaTiO_3$ ceramics with cerium doping, manganese doping and Ce-Mn co-doping. Sci Eng Compos Mater. 2019; 26:62–9. https://doi.org/10.1515/secm-2017-0177
3. Yao FZ, Yuan O, Wang Q, Wang H. Multiscale structural engineering of dielectric ceramics for energy storage applications: from bulk to thin films. Nanoscale. 2020; 12:17165-84. https://doi.org/10.1039/D0NR04479B
4. Panda M, Mishra A, Shukla P. Efective enhancement of dielectric properties in coldpressed polyvinyledene fuoride/barium titanate nanocomposites. SN Applied Sciences. 2019; 1:230. https://doi.org/10.1007/s42452-019-0234-9
5. Uk. P. Reports, SpeciPaul O'Brien, University of Manchester, Nanoscience 1: Nanostructures through Chemistry. vol. DOI: 10.10. 2013.
6. Kasian P, Thongbai P, Yamwong T, Rujirawat S, Yimnirun R, Maensiri S. The DC bias voltage effect and non-linear dielectric properties of titanate nanotubes. J Nanosci Nanotech. 2015; 15(11):9197–202. https://doi.org/10.1166/jnn.2015.11406
7. Taeseok K, Jeongmin O, Byungwoo P, Kug Sun H. Dielectric properties and strain analysis in paraelectric $ZrTiO_4$ thin films deposited by DC magnetron sputtering. Jpn J Appl Phys. 2000; 39:4153–7. https://doi.org/10.1143/JJAP.39.4153
8. Viticoli M, Padeletti G, Kaciulis S, Ingo GM, Pandolfi L, Zaldo C. Structural and dielectric properties of $ZrTiO_4$ and $Zr_{0.8}Sn_{0.2}TiO_4$ deposited by pulsed laser

deposition. Materials Science and Engineering B. 2005; 118:87–91. https://doi:10.1016/j.mseb.2004.12.047
9. Newnham RE. Am Cer Soc. 1967; 50:216. https://doi.org/10.1038/scientificamerican0667-50
10. Al-Azawi MA, Bidin N. Gold nanoparticles synthesized by laser ablation in deionized water. Chinese Journal of Physics. 2015; 53(4). https://doi:10.6122CJP.20150511B.
11. Asanithi P, Chaiyakun S, Limsuwan P. Growth of silver nanoparticles by DC magnetron sputtering. Journal of Nanomaterials. 2012; 963609:8. https://doi.org/10.1155/2012/963609
12. Carneiro JO, Azevedo S, Fernandes F, Freitas E, Pereira M, Tavares CJ, Lanceros-Me´ndez S, Teixeira V. Synthesis of iron-doped TiO_2 nanoparticles by ball-milling process: the influence of process parameters on the structural, optical, magnetic, and photocatalytic properties. J Mater Sci. 2014; 49:7476–88. https://doi.org/10.1007/s10853-014-8453-3
13. Hu XL, Takai O, Saito N. Synthesis of gold nanoparticles by solution plasma sputtering in various solvents. Journal of Physics: Conference Series. 2013; 417:012030. https://doi.org/10.1088/1742-6596/417/1/012030
14. Virk HS, Sharma P. Chemical route to nanotechnology. International Journal of Advanced Engineering Technology. IJAET. 2010; 1(3):114-29.
15. Sangeetha A, Sathish KN, Nagabhushana BM, Chikkahanumantharayappa, Jayasankar CK. Red, Green, Blue and IR emitting zirconium Titanate nano composite co-doped with $Er^{3+}/Tm^{3+}/Yb^{3+}$ synthesized by combustion synthesis. Optical Materials. 2021; 121:111534. https://doi.org/10.1016/j.optmat.2021.111534
16. Sangeetha A, Chikkahanumantharayappa, Nagabhushana BM. Comparative study of photoluminescence of single and mixed phase $ZrTiO_4$ prepared by solution combustion and polymeric precursor method. Journal of Molecular Structure. 2019; 1179:126e131. https://doi.org/10.1016/j.molstruc.2018.10.059
17. Verma S, Rani S, Kumar S, Majeed Khan MA. Rietveld refinement, micro-structural, optical and thermal parameters of zirconium titanate composites. Ceramics International. 2018; 44(2):1653-61. https://doi.org/10.1016/j.ceramint.2017.10.090
18. Xu J, Lind C, Wilkinson AP, Pattanik S. X-Ray diffraction and X-ray absorption spectroscopy studies of sol-gel processed zirconium titanate. Chem Mater. 2000; 12:3347-55. https://doi.org/10.1021/cm000298s
19. Victor P, Bhattacharyya S, Krupanidhi SB. Dielectric relaxation in laser ablated polycrystalline $ZrTiO_4$ thin films. Journal of Applied Physics. 2003; 94:5135. https://doi.org/10.1063/1.1606509
20. Kim D-S, Park D-H, Kim G-D, Choi S-Y. Dielectric Properties of $ZrTiO_4$ Thin Films Synthesized by Sol-Gel Method. Metals and Materials International. 2004; 10(4):361-5. https://doi.org/10.1007/BF03185986
21. Yugandhar B, Dastagiri S, Manjunath V, Lakshmaiah MV. Structural and dielectric properties of $Pb_xZr_{1-x}TiO_4$ (x=0.1- 0.4) ceramics by solid state reaction method. International Journal of Scientific and Engineering Research. 2019; 10(7). http://www.ijser.org
22. Dey B, Narzary R, Chouhan L, Bhattacharjee S, Parida BN, Mondal A, Ravi S, Srivastava SK. Crystal structure, optical and dielectric properties of Ag:ZnO composite-like compounds. J Mater Sci: Mater Electron. https://doi.org/10.1007/s10854-021-07560-4
23. Sahu G, Das M, Yadav M, Sahoo BP, Tripathy J. Dielectric relaxation behavior of silver nanoparticles and graphene oxide embedded poly(vinyl alcohol) nanocomposite film: an effect of ionic liquid and temperature. Polymers. 2020; 12(2):374. https://doi.org/10.3390/polym12020374
24. Mohanty B, Parida BN, Parida RK. Mater Chem Phys. 2019; 225:91–8. https://doi.org/10.1016/j.matchemphys.2018.12.076